THE JOURNAL OF PHYSICAL CHEMISTRY C
A JOURNAL OF THE AMERICAN CHEMICAL SOCIETY

pubs.acs.org/JPCC

Article

Giant Effects of Interlayer Interaction on Valence-Band Splitting in Transition Metal Dichalcogenides

Garrett Benson, Viviane Zurdo Costa, Neal Border, Kentaro Yumigeta, Mark Blei, Sefaattin Tongay, K. Watanabe, T. Taniguchi, Andrew Ichimura, Santosh KC, Taha Salavati-fard, Bin Wang, and Akm Newaz*

Cite This: J. Phys. Chem. C 2022, 126, 8667−8675

Read Online

ACCESS | Metrics & More | Article Recommendations | Supporting Information

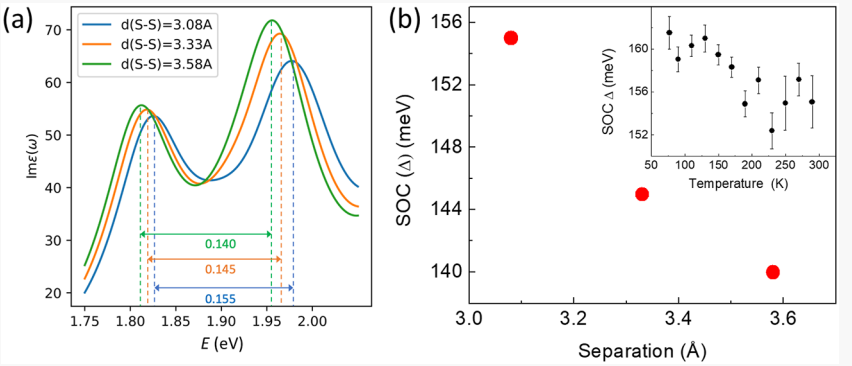

ABSTRACT: Understanding the origin of valence band maxima (VBM) splitting in transition metal dichalcogenides (TMDs) is important because it governs the unique spin and valley physics in monolayer and multilayer TMDs. In this work, we present our systematic study of VBM splitting (Δ) in atomically thin MoS_2 and WS_2 by employing photocurrent spectroscopy. We found that VBM splitting in monolayer MoS_2 and WS_2 depends strongly on temperature, which contradicts the theory that spin−orbit coupling solely determines the VBM splitting in a monolayer TMD. We also found that the rate of change of VBM splitting with respect to temperature ($m = \frac{\partial \Delta}{\partial T}$) is the highest for monolayer (−0.14 meV/K for MoS_2) and the rate decreases as the layer number increases ($m \approx 0$ meV/K for 5 layers MOS_2). Our density functional theory (DFT) and the GW with Bethe−Salpeter Equation (GW-BSE) simulations agree with the experimental observations and demonstrate that the temperature dependence of VBM splitting in monolayer and multilayer TMDs originates from the changes in the interlayer coupling strength between the neighboring layers and substrates. We also found that VBM splitting depends on the layer numbers and the type of transition metals.

INTRODUCTION

Transition metal dichalcogenides (TMDs) exhibit remarkable properties resulting from their reduced dimensionality and crystal symmetry.[1−6] Monolayer TMDs (1L-TMDs) have a direct band gap at the K point of the Brillouin zone, which is different from its corresponding few-layer and bulk counterparts with indirect band gaps.[1−6] The valence band maxima (VBM) at the K point in TMDs split, which is attributed to the large spin−orbit coupling (SOC) in 1L-TMDs and the mixing of SOC and interlayer coupling for multilayer TMDs.[7−13] Strong SOC in TMDs originates from the *d*-orbitals of the heavy transition-metal atoms.[7] Unique crystal symmetry of TMDs causes coupling of spin and valley degrees of freedom.[14] The crystal symmetry of TMDs and SOC cause a sizable split (Δ > 100 meV) in the valence band at the K point in the Brillouin Zone (BZ). This large splitting governs many observable physical phenomena such as the spin-Hall effect,[15] valley-Hall effect,[16] and optical circular dichroism.[17]

Despite the importance of the VBM splitting that causes the unique spin and valley physics of TMDs, the temperature and layer dependence of VBM splitting have not been well studied experimentally. In this work, we present our systematic study of VBM splitting in MoS_2 and WS_2 as we change the temperature and the layer number by employing photocurrent spectroscopy. Surprisingly, we observed that the VBM splitting in 1L-TMDs depends on the temperature, which contradicts the theory that VBM splitting in 1L-TMDs originates solely from the SOC. Our finding also contradicts two previously

Received: December 16, 2021
Revised: April 29, 2022
Published: May 13, 2022

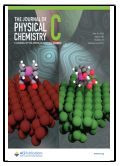

https://doi.org/10.1021/acs.jpcc.1c10631
J. Phys. Chem. C 2022, 126, 8667−8675

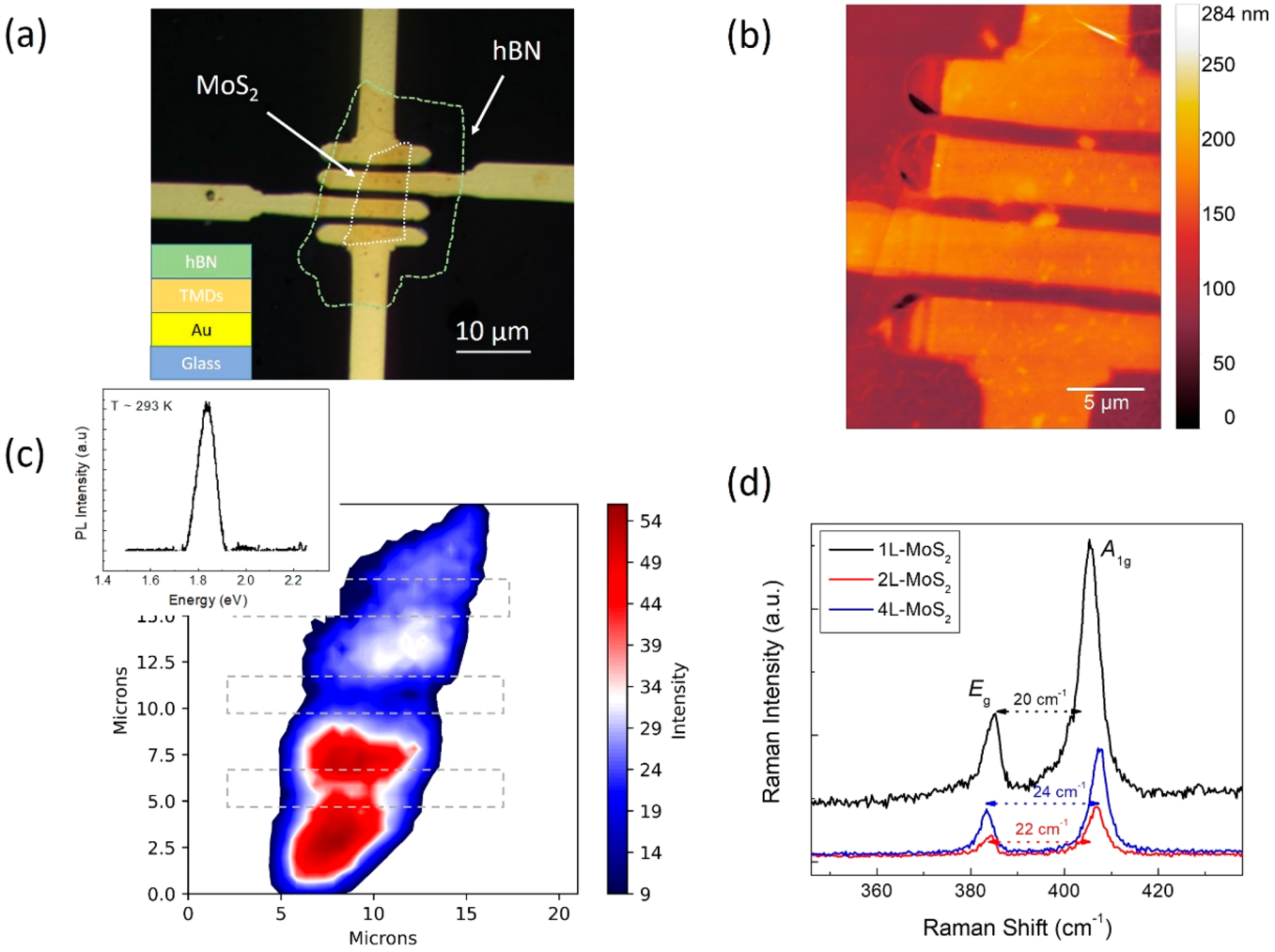

Figure 1. (a) Optical image of a 1L-MoS_2 sample connected to Au electrodes (yellow). The MoS_2 flake is marked by the dashed white line. The MoS_2 samples are covered by a few-layer hBN flake marked by a green dashed line. The left inset is showing the vertical structure of the sample schematically. (b) An AFM image of the same sample. (c) The photoluminescence mapping of the sample at room temperature. This is a spatial contour plot showing the integrated PL intensity for different locations of the laser beam on the sample. The inset is showing a PL spectrum from the sample. The gray-colored dashed boxes show the location of the Au electrodes. The laser excitation wavelength was 532 nm. We see the A-exciton peak at 1.83 eV, a characteristic of a 1L-MoS_2 sample. The parallel structure in the mapping image is arising from the Au electrode induced PL quenching. (d) Raman spectrum of three different layer MoS_2 samples (monolayer, bilayer, and 4-layers). The peak separation between E_g and A_{1g} are also shown. The excitation laser source was 532 nm.

reported experimental studies that concluded that the VBM splitting in monolayer TMDs originates from SOC only.[13,18] Intriguingly, we found that the temperature dependence is the strongest for 1L-MoS_2 than multilayer MoS_2. We also found that VBM splitting in TMDs (MoS_2 and WS_2) depends on the layer numbers and type of transition metals. We calculated the electronic band structure of bilayer MoS_2 by using density functional theory (DFT) and determined the absorption spectra using the GW-BSE approach, which agrees with experimentally measured VBM properties in MoS_2.

MATERIALS AND METHODS

Sample Fabrication. We prepared MoS_2 flakes from a naturally grown Molybdenite rock. The WS_2 samples were grown by chemical vapor transport (CVT) technique. We exfoliated MoS_2 and WS_2 flakes from bulk crystals onto a thermally grown SiO_2 film on a heavily doped Si wafer. Before the mechanical transfer of TMD flakes, the wafers were cleaned by acetone and isopropanol. The wafers were manufactured by Silicon Valley Microelectronics. The MoS_2 and WS_2 layers were characterized by using optical microscopy, Raman spectroscopy, and AFM. For encapsulation with a few layers of hBN, we prepare hBN flakes on SiO_2/Si substrate, which was picked by polyethylene terephthalate (PET). We used a PET stamp to pick up the top hBN flake, atomically thin TMDs in sequence with accurate alignment using a homemade transfer stage. The hBN/TMDs heterostructure was then stamped on a prefabricated Au electrode (90 nm Au/5 nm Cr) on a glass substrate. We used alkaline earth boro-aluminosilicate glasses, which were bought from the Delta Technologies (see Supporting Information for details). The patterned Au electrodes were fabricated using optical lithography followed by thermal evaporation of metals. All devices were Fabricated on a glass substrate to avoid the photogating effect.[19−21]

Raman Characterization. Confocal micro-Raman measurements were performed using commercial equipment (Horiba LabRAM Evolution). A 100× objective lens with a

https://doi.org/10.1021/acs.jpcc.1c10631
J. Phys. Chem. C 2022, 126, 8667−8675

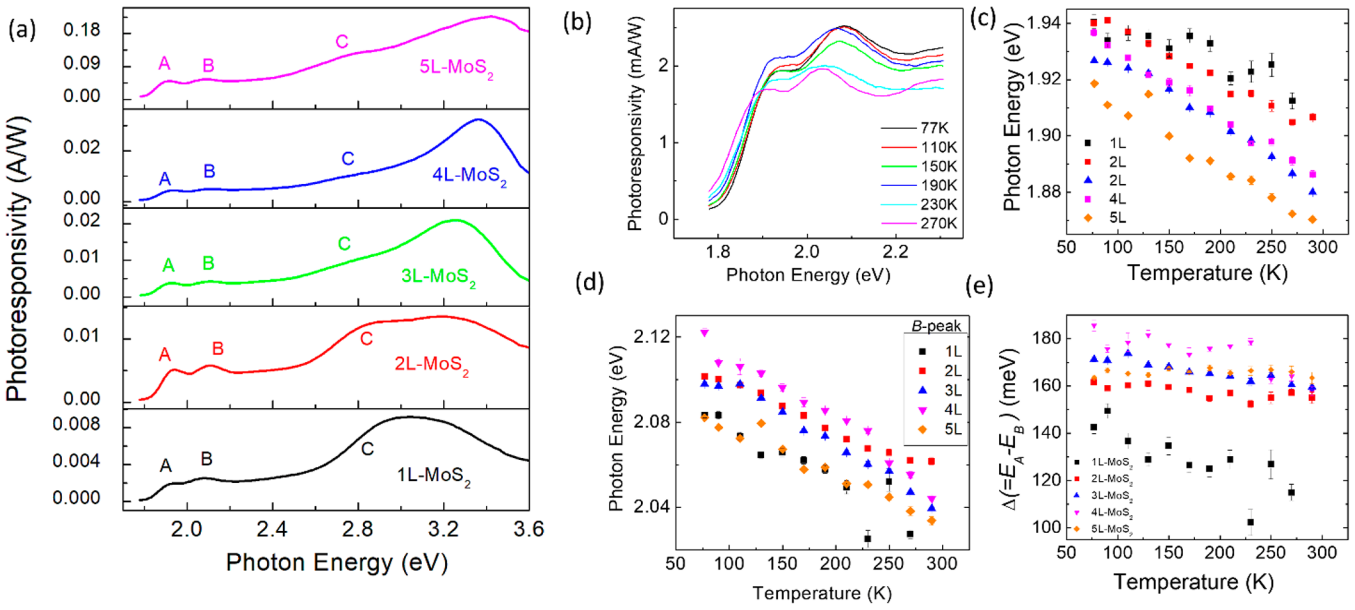

Figure 2. VBM splitting of MoS_2. (a) Photocurrent spectra of different layered MoS_2 (1L to 5L). The left axis is presenting the photoresponsivity. (b) Photoresponsivity of a 1L-MoS_2 sample at different temperatures. (c) The plot is showing the A-peak position at different temperatures for different layered thicknesses. (d) The plot is showing the B-peak position at different temperatures for different layered thicknesses. (e) The difference between the energy of the A and B peaks or VBM splitting Δ at different temperatures.

numerical aperture of 0.9 was used. The excitation source was a 532 nm laser (2.33 eV) with an optical power of ∼170 μW.

Laser Assisted Thermal Annealing. To obtain lower contact resistance, we annealed the devices using a 532 nm laser of beam power ∼200 mW. The beam diameter is ∼2 μm. We kept the devices at 77 K, and under a bias voltage while we annealed the devices. The bias voltages were varied depending on the devices to obtain a measurable current. After annealing for 2 min, we measure the photocurrent spectroscopy. If the signal-to-noise ratio in photocurrent is low, we repeated the laser assisted annealing process. We continued the process until we obtained a high signal to low noise ratio.

Photocurrent Spectroscopy. The photocurrent spectroscopy (PCS) at a varying temperature from 77 to 300 K was conducted using a microscopy cryostat (Janis Research). We illuminate devices using a low-intensity broad-band white light from a thermal light source and record photocurrent generated from the device across a range of photon wavelengths. The optical beam from the broad-band thermal source (quartz halogen lamp) was directed through a monochromator (Acton Pro SP-2150i) and a mechanical chopper (45 Hz) onto the sample where it was focused down to a spot (∼10 μm) with a diameter larger than the device. The photocurrent was measured by using a preamplifier (Stanford Research, SR570) connected to a lock-in-amplifier (Stanford Research, SR-830), which was locked to the chopping frequency. A commercial silicon photodetector (Hamamatsu S1223) was used to calibrate the light intensity incident on the sample.

DFT Calculations. The DFT calculations were performed using the Vienna *ab initio* simulation package (VASP).[22,23] The nuclei and core electrons were described by the projector augmented wave function (PAW).[24,25] The exchange-correlation used was the generalized gradient approximation (GGA) of the Perdew–Burke–Ernzerhof (PBE) functional. All the structures were optimized until the maximum Hellmann–Feynman forces acting on each atom and the total energy is less than 0.01 eV/Å and 10^{-5} eV, respectively. Each slab has a vacuum thickness of 20 Å along the *z*-direction to avoid the interaction due to periodic boundary conditions.

We used the GW-BSE method to calculate the absorption spectrum of TMDs.[26] The GPAW electronic structure calculations software,[27,28] version 21.6.0, was employed to calculate the dielectric functions of the studied systems. Using the imaginary part of the dielectric function, optical adsorption spectrum and excitonic A and B peaks within the GW-BSE level of theory, which includes electron–hole correlations, were obtained. The reciprocal space was sampled by a highly fine 30 × 30 × 1 k-points grid, and truncated Coulomb interaction was considered to decouple the screening between periodic images.[29] The cutoff energy for the response function was set to 50 eV. The four highest energy bands below and the four lowest energy bands above the Fermi level were included in the GW-BSE calculations.

RESULTS AND DISCUSSION

To probe VBM splitting in atomically thin semiconductors, we fabricated molybdenum disulfide (MoS_2) and tungsten disulfide (WS_2) flakes that are electrically connected for transport measurement. All the samples reported here are covered by hexagonal boron nitride (hBN) for environmental protection. The MoS_2 and WS_2 flakes were mechanically exfoliated from bulk crystals onto a heavily doped silicon substrate capped with a 90 nm thick thermally grown SiO_2 film. The MoS_2 flakes were obtained from naturally grown rock, and WS_2 samples were grown by a chemical vapor transport (CVT) technique. The number of TMD layers was characterized by using optical microscopy and Raman spectroscopy. Atomic force microscopy (AFM) was performed in AC mode (JPK NanoWizard, Tap300Al-G cantilever) to confirm the topography of the monolayer specimens.

To protect the TMDs, few-layer hBN flakes were deposited on the SiO_2/Si substrate, which was picked up by a polyethylene terephthalate (PET) stamp. After the top hBN flake adhered to the PET, the stamp was placed on atomically

https://doi.org/10.1021/acs.jpcc.1c10631
J. Phys. Chem. C 2022, 126, 8667−8675

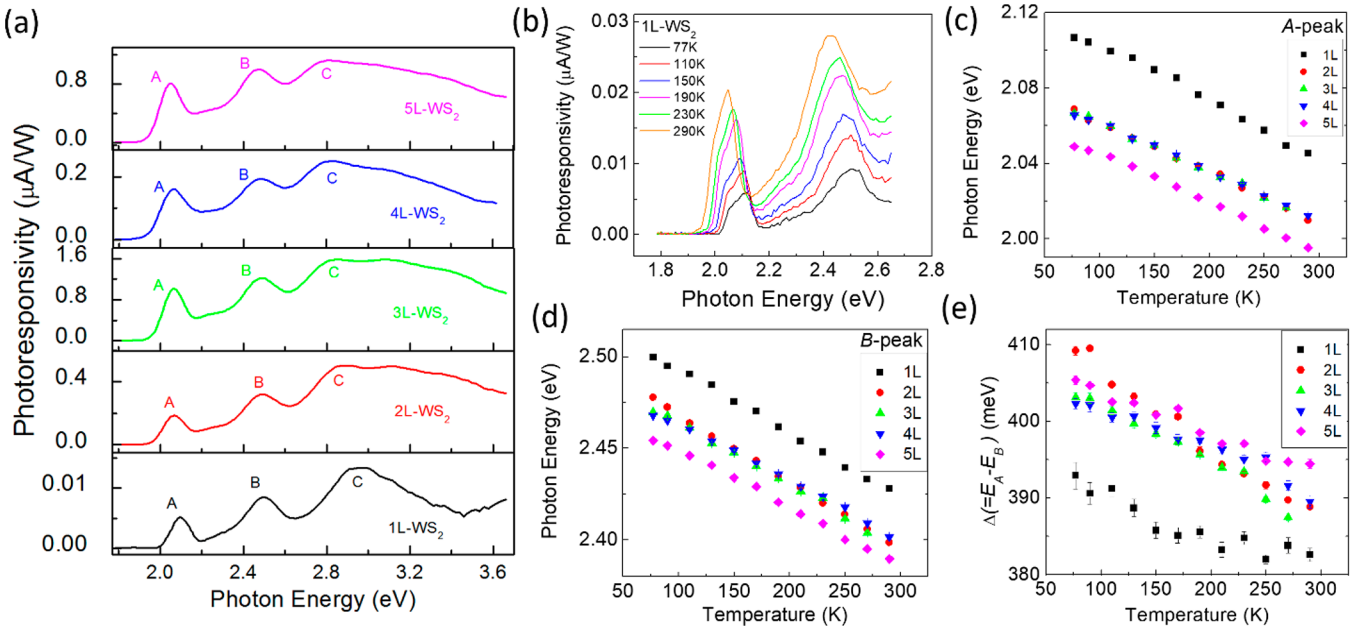

Figure 3. VBM splitting of WS_2. (a) Photocurrent spectra of different layered WS_2 (1L to 5L). The left axis is presenting the photoresponsivity. (b) Photoresponsivity of a 1L-WS_2 sample at different temperatures. (c) The plot is showing the A-peak position at different temperatures for different layered thicknesses. (d) The plot is showing the B-peak position at different temperatures for different layered thicknesses. (e) The difference between the energy of the A and B peaks, or VBM splitting Δ at different temperatures for different thicknesses from 1L to 5L.

thin TMDs with accurate alignment using an optical microscope. The hBN/TMDs heterostructure was then stamped on a prefabricated Au electrode (90 nm Au/5 nm Cr) on a glass substrate (see Methods and Supporting Information for details). The patterned Au electrodes were fabricated using optical lithography followed by thermal evaporation of metals.

Figure 1a shows the optical images of a monolayer MoS_2 device encapsulated or covered by an hBN layer. The vertical design of the heterostructure sample is shown schematically in the Figure 1a inset. The AFM image of the sample is shown in Figure 1b. We conducted photoluminescence (PL) scanning of the sample at room temperature and created a spatial contour plot, as shown in Figure 1c, by plotting the integrated PL intensity for different laser positions on the sample. A representative PL spectrum is shown in the inset of Figure 1c. The PL spectrum shows a large peak at 1.8 eV due to the A-exciton, which is characteristic of 1L-MoS_2.[30] Figure 1d compares the Raman spectra for 1L, 2L, and 4L-MoS_2 samples and the difference in energy between the A_{1g} and E_g peaks.

Reduced screening and strong light−matter interactions in van der Waals (vdWs) materials cause the formation of a wide range of many-body excitonic states. Intralayer excitons are bound electron−hole ($e-h$) pairs in the same layers, such as A/B excitons in TMDs originating from the split VBM at the K point. Hence, the measurement of A and B excitons provide a direct pathway to measure the VBM splitting. In addition to these many-body bound states, the band structure of 1L-TMDs causes a singularity in the joint density of states (JDoS) resulting in a unique exciton type, known as van Hove singularity excitons, also known as C and D excitons.[19,31]

To measure the VBM splitting directly, we conducted photocurrent spectroscopy (PCS) as a function of temperature from 77 to 300 K using a microscopy cryostat. We annealed every device using a 532 nm high power laser (~200 mW) while the device was kept at 77 K inside the cryostat (see Methods for details). We illuminate devices using a low-intensity broad-band white light from a thermal light source and record photocurrent generated from the device across a range of photon wavelengths (see Methods for details). In total, we studied 13 MoS_2 devices and 13 WS_2 devices (see Supporting Information for details).

Figure 2a presents the photocurrent spectroscopy for 1L−5L MoS_2 samples measured at 77 K. We observed clearly A, B, and C peaks in the spectrum as marked in Figure 2a. We also observed a small peak between B and C peaks, whose origin is not clear and beyond the scope of the paper. Further study is necessary to identify this new peak.

We present the photocurrent data in terms of photoresponsivity (i.e., the photocurrent generated per unit of optical power). To collect the photocurrent, we biased the devices with different bias voltages ranging from 1 to 10 V using a source-meter (Keithley 2400). PC spectroscopy (PCS) is very similar to absorption spectroscopy because both are direct absorption processes, which allows the study of single- and many-body electronic states and valence band splitting in TMDs.[19] Unlike absorption spectroscopy, PCS of 1L- 5L TMDs can be easily measured for an electrically contacted microscopic device within a cryogenic environment, as the device itself acts as its own photodetector.

The separation between peaks A and B in the photocurrent spectra directly measures the VBM splitting in TMDs. We used Lorentzian fitting to determine the A and B peak positions and the corresponding errors of the peak position. Figure 2b presents the energy-resolved photoresponsivity spectra at temperatures ranging from 77 to 270 K. We see that A and B peaks red-shift as the temperature increases. The A and B peak positions of 1L−5L MoS_2 samples as a function of temperatures are shown separately in Figure 2c and 2d, respectively. We calculated VBM splitting from the difference between A and B peaks as shown in Figure 2e (error bars were determined by the propagation of error).

https://doi.org/10.1021/acs.jpcc.1c10631
J. Phys. Chem. C 2022, 126, 8667−8675

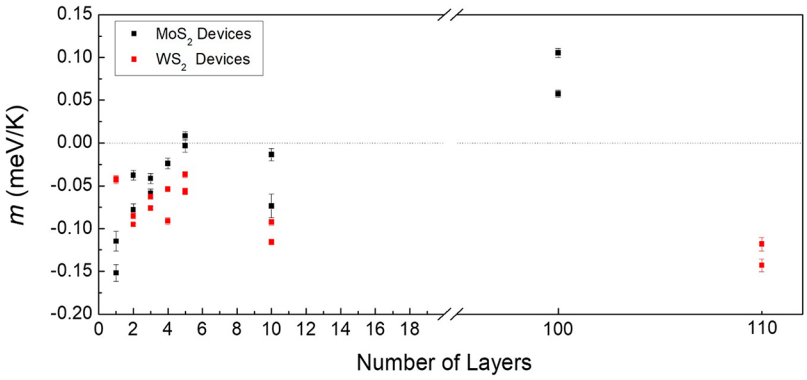

Figure 4. Rate ($m = \frac{\partial(E_A - E_B)}{\partial T}$) at which the splitting is behaving as we change the temperature for different layers MoS_2 and WS_2. For a blow-up view of the splitting changing rate for 1L to 5L, a break in the *x*-axis is used. The error bars are also indicated.

The temperature-dependent VBM splitting strength Δ (= $E_B - E_A$, where E_A and E_B are the peak positions of the A and B peak, respectively) for different layered flakes reveals three important features. First, we observed that VBM splitting in 1L-MoS_2 strongly depends on temperature. This is very surprising, as the current theory indicates that VBM splitting in 1L-TMDs originates from the spin−orbit coupling only, which should be temperature-independent, as SOC is a relativistic effect. Second, the rate of change of the coupling strength ($m = \frac{\partial \Delta}{\partial T}$) depends on the layer thickness. It is the highest for a monolayer MoS_2 (−0.14 meV/K) and it reduces to vanishingly small for 5L-MoS_2. Interestingly, we found that the rate becomes positive (0.08 meV/K) for bulk (∼100 layers) MoS_2. Third, the VBM splitting value is lowest for monolayer and increases as we increase the layer thickness.

Recently Zhang et al.[13] demonstrated the temperature-dependent properties of VBM splitting in MoS_2 by using photoluminescence (PL) spectroscopy. Though the reported results are interesting, we argue that their conclusions are heavily affected by two characteristics of PL measurements. First, the B peak intensity in PL measurements is weak compared to the A-peak, which makes it challenging to pinpoint the B peak energy and determine the VBM splitting. Second, PL is a second-order process in which the TMD first absorbs the photon exciting electrons from the valence band to the conduction band, and then reemits a photon as the electron transitions to the valence band. On the other hand, PCS is a more precise technique to determine the VBM splitting than PL spectroscopy because PCS is a direct photon process that provides equally strong A and B peaks. We measured properties of VBM splitting in TMDs that are significantly different than the results reported by Zhang et al.[13] In particular, we found strong temperature-*dependent* VBM splitting in 1L- and 2L-TMDs, whereas Zhang et al. demonstrated temperature-*independent* VBM splitting for 1L- and 2L-MoS_2.

To understand the effect of the transition-metal ions in VBM splitting, we also studied VBM splitting in WS_2 by using photocurrent spectroscopy at varying temperatures and layer numbers. We studied samples of different thicknesses ranging from a monolayer (1L) to five layers (5L). Figure 3a presents the photocurrent spectroscopy data recorded at 77 K for 1L−5L samples.

Figure 3b shows the photocurrent spectra at different temperatures for a monolayer WS_2 sample (see Supporting Information for the details of the sample). Interestingly, the photoresponsivity increases with increasing temperature. We attribute this effect to the lower resistance of the devices with increasing temperature. Figure 3c and 3d present the positions of WS_2 A and B peaks, respectively, at different temperatures. The peak positions and the corresponding errors were determined by fitting to a Lorentzian function. Figure 3e presents the VBM splitting as a function of temperature.

We observed three interesting features in the VBM splitting-temperature plots of WS_2. First, VBM splitting, Δ, decreases as we increase the temperature. The reduction of Δ in 1L-WS_2 confirms that the splitting is not originating solely from SOC similar to the case in 1L-MoS_2 as shown in Figure 2e. Second, the rate of change of Δ with respect to temperatures remains independent of layer thickness, which is different than the trend observed for MoS_2. Finally, the VBM splitting in monolayer WS_2 has the smallest value and it increases for multilayer WS_2.

To quantify the temperature-dependent change of VBM splitting, we calculated the rate of change $m = \frac{\partial \Delta}{\partial T}$, for all the samples. We also studied a bulk MoS_2 sample (layer number ∼100 determined by AFM thickness measurement) and a bulk WS_2 sample (layer number ∼110). The calculated rate *m* for all the samples studied in this experiment is shown in Figure 4. It is evident from the plot that the rate *m* for MoS_2 increases as the layer number increases up to 5L. Interestingly, we did not observe any clear trend for WS_2 samples depending on the layer thickness. For the bulk sample, *m* becomes positive for MoS_2, whereas *m* remains negative for WS_2. For two 10-layer MoS_2 samples, we observed widely separated *m* values, whose origin is not clear to us.

It has been argued that the VBM splitting can be attributed entirely to SOC at the monolayer limit,[7−13] which suggests that the Δ in 1L-TMDs should be independent of temperature. Instead, we observed the strongest temperature-dependent VBM splitting for monolayer MoS_2 compared to a few or higher number of layers. Our result suggests that the VBM splitting at the monolayer limit is not due solely to SOC. Note that our 1L-TMD samples are in contact with the top hBN layer and bottom glass substrate. The contact length between 1L-TMDs and the glass substrate is ∼500 nm (see Supporting Information for details). Since we used the top hBN layer as an encapsulation, it is in full contact with the top side of the sample. We argue that the VBM splitting of 1L-MoS_2 originates from the combination of SOC and the interaction

https://doi.org/10.1021/acs.jpcc.1c10631
J. Phys. Chem. C 2022, 126, 8667−8675

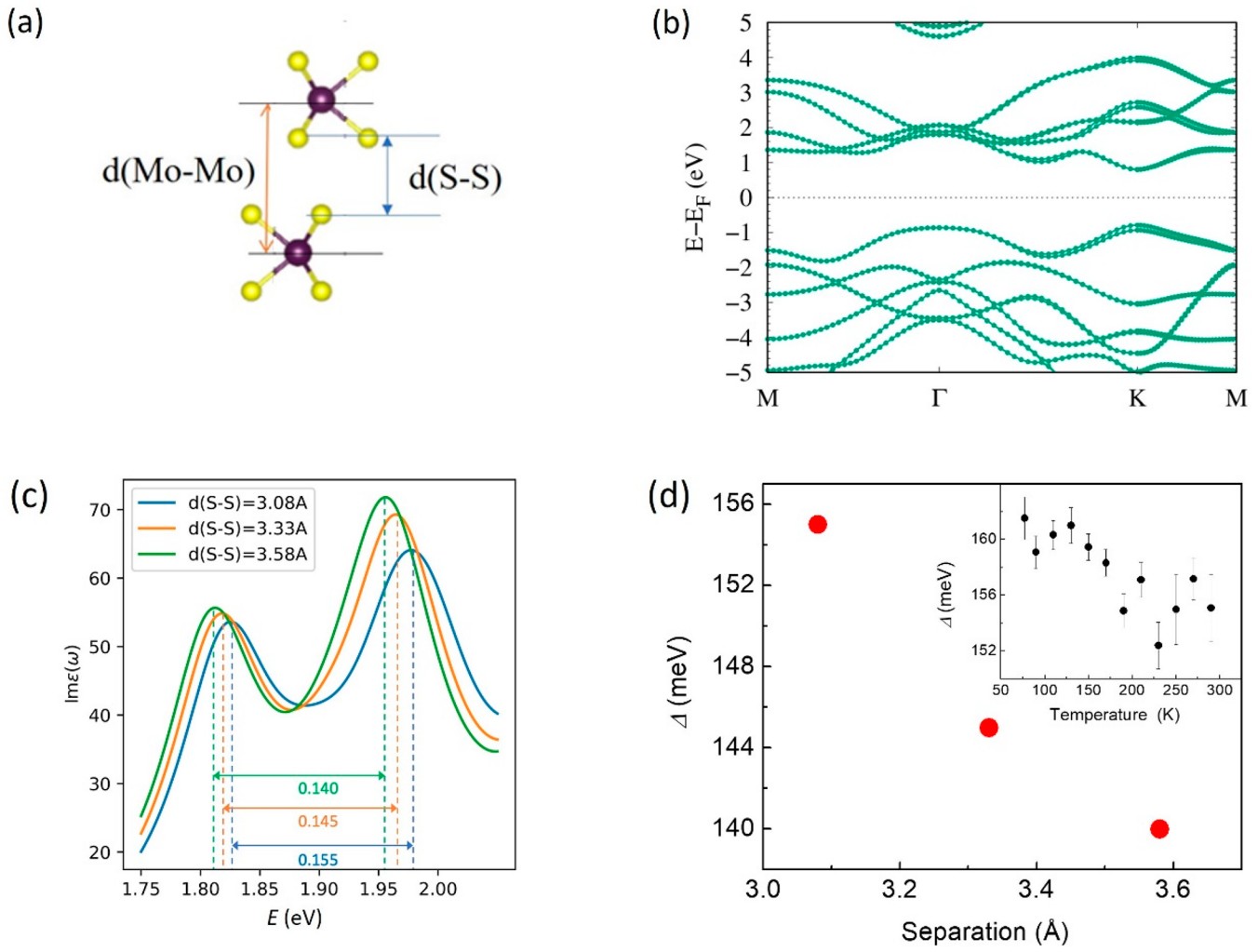

Figure 5. (a) Optimized atomic structure of a bilayer MoS_2. (b) Calculated electronic band structure with spin−orbit coupling. (c) Absorption spectra for different interlayer d(S−S) separation for d_0 = 3.08 Å, d_1 = 3.33 Å, and d_2 = 3.58 Å. (d) Comparison of calculated VBM splitting values of a bilayer MoS_2 with the experimentally measured values. The main panel shows the calculated VBM splitting values for different interlayer separations. The inset is presenting experimentally measured VBM splitting for a 1L-MoS_2 as we change the temperature. The experimental results are the same data set presented in Figure 2e.

of the TMD with the top hBN layer and bottom glass substrate.

When a TMD is subjected to out-of-plane compressive pressure, it has been shown that the interlayer separation between the adjacent TMD layer (δ) decreases and the interlayer interaction between the layer increases.[18,32] It has also been demonstrated that the Raman active vibrational modes (both E_g and A_{1g} modes) blue-shift as the pressure is increased,[33] which suggests that the blue shift (red shift) of the Raman peak is a signature of the decrease (increase) of interlayer separation δ and increase (decrease) of interlayer interaction. Since an increase in temperature causes a red shift of both E_g and A_{1g} Raman peaks,[34] the average interlayer separation δ increases, and interlayer interaction decreases as one increases the temperature. Hence, we argue that the observed temperature-dependence of VBM splitting in TMDs is originating from the change in the interlayer separation that affects the interlayer coupling strength.

The valence band splitting is mainly due to spin−orbit coupling and partly due to interlayer interaction.[9,12,35] The interlayer coupling in TMDs arises from the weak van der Waals force between neighboring layers or substrates. Even though van der Waals interaction is relatively weak, small changes in the distance between adjacent layers can significantly change the conduction and valence band minimum and maximum, respectively, as well as the vibrational properties of layered materials.[36,37] It has been demonstrated that this change is linked to the strong out-of-plane hybridization effects and van der Waals interactions.[36,37]

For bilayer and multilayer TMDs, the interlayer distance increases as the temperature is increased, which causes a shift in the energy of the out-of-plane vibration modes[34] and reduces the strength of the van der Waals interaction. In addition, the interlayer out-of-plane coupling of Mo d orbitals ($d_{z^2} - d_{z^2}$) will affect the spin orbit coupling strength of the valence band.

When we have a single layer 1L-MoS_2 or 1L-WS_2 residing on a glass substrate and encapsulated by hBN, the surfaces interact with the S atoms of MoS_2. The sulfur−substrate and sulfur−hBN interaction introduces anisotropy of Mo−S hybridization along the out-of-plane direction. Since Mo d- and S p-orbital hybridization contribute to the valence band edge, the interaction with the substrate and hBN will modify the spin orbit coupling strength, which will be reflected in VBM

https://doi.org/10.1021/acs.jpcc.1c10631
J. Phys. Chem. C 2022, 126, 8667−8675

splitting.[38] Moreover, the dielectric screening is also modified by the interlayer interactions.[39] Thus, the change in the interlayer distance due to temperature affects the VBM splitting as well as the observed band gap.

To understand the effect of interlayer separation on VBM splitting, we conducted DFT and GW-BSE calculations to determine the band structure and absorption spectra. In a TMD monolayer, there will be a combined effect of substrate/hBN dielectrics that is more pronounced for the monolayer due to the reduced dimension and temperature effect. Moreover, the variability of the interface structure, effect of substrate strain, and dielectric screen effect with temperature is challenging and computationally expensive and requires effort beyond DFT.[40,41] For these reasons, we conducted calculations for only a bilayer MoS_2 as a function of interlayer separation. The optimized atomic structure of a bilayer MoS_2 is shown in Figure 5a.

We simulated the electronic band structure using the DFT calculations. The calculations were performed using the Vienna *ab initio* simulation package (VASP).[22,23] See Methods section for details. The electronic band structure calculated by DFT methods shows the VBM splitting at the K point of the Brillouin zone (Figure 5b).

To understand the excitonic A−B peak difference as a function of the interlayer separation of a bilayer MoS_2, we employ the GW-BSE method.[26] See Methods section for details. Including the relativistic effect, the VBM splitting is 155 meV in 2L-MoS_2 for a sulfur−sulfur distance of d(S−S) = 3.08 Å. The calculated absorption spectra for three different values of d(S−S) = 3.08 Å, 3.33 Å, and 3.58 Å are shown in Figure 5c. As we increase the interlayer separation, Δ (VBM) decreases as shown in Figure 5d. The inset of Figure 5d shows the experimentally determined Δ values for 2L-MoS_2 for comparison.

Since we measured Δ experimentally as a function of the temperature and calculated Δ as a function of interlayer separation, we can only make a qualitative comparison. Our results clearly demonstrate that the temperature dependence of Δ originates from the change in interlayer separation or interlayer interaction strengths. We observed that Δ for a bilayer MoS_2 varies by ∼10 meV as we change the temperature from 77 to 300 K. Interestingly, our simulations also predict that the change in Δ has a very similar magnitude when compared to our experiments as the interlayer separation is increased by 0.25 Å. We note that there is an ∼10 meV offset value between experimental measurements and simulations, but the trend still provides an explanation for the experimentally observed temperature dependence of VBM splitting.

We note here that studying the interlayer interaction on the valence band-splitting for a monolayer TMDs on different substrates will further clarify the effect. But that study is beyond the scope of this current manuscript. We will study the interlayer interaction effect for 1L-TMDs residing on different substrates and will report the results in a future publication.

CONCLUSIONS

In conclusion, we studied temperature-, layer-, and material-dependent VBM splitting for two different types of TMDs using photocurrent spectroscopy. We found that the VBM splitting depends on temperature, thickness, and materials of atomically thin TMDs. Our finding of VBM splitting in 1L-TMDs depending on temperature indicates that splitting Δ in 1L-TMDs does not originate solely from the SOC coupling. This result suggests that either SOC in 1L-TMDs is temperature-dependent or VBM splitting in 1L-TMDs is governed by the combination of SOC and coupling strength to the neighboring surface or the substrate. Since SOC is a relativistic effect, we argue that VBM splitting in 1L-TMDs is caused by the combination of SOC and the interaction with the neighboring surfaces. We also found that the rate of change of VBM splitting with respect to temperature is the highest for the monolayer and the rate decreases as the layer number increases. To understand the effect, we calculated the electronic band structure and VBM splitting for a bilayer with different interlayer separations, which suggests that the temperature-dependent VBM splitting in atomically 2L-TMDs can originate from the changes in the interlayer separation between neighboring layers. Our study will help understand the intricate role spin−orbit coupling and interlayer interactions play in determining the VBM splitting in quantum materials.

ASSOCIATED CONTENT

Supporting Information

The Supporting Information is available free of charge at https://pubs.acs.org/doi/10.1021/acs.jpcc.1c10631.

Prepatterned Au electrodes Fabrication, Monolayer WS2 sample characterization, Determination of contact length between the glass substrate and TMDs, and Device information (PDF)

AUTHOR INFORMATION

Corresponding Author

Akm Newaz − *Department of Physics and Astronomy, San Francisco State University, San Francisco, California 94132, United States;* orcid.org/0000-0001-8159-1604; Phone: 415-338-2944; Email: akmnewaz@sfsu.edu

Authors

Garrett Benson − *Department of Physics and Astronomy, San Francisco State University, San Francisco, California 94132, United States*

Viviane Zurdo Costa − *Department of Physics and Astronomy, San Francisco State University, San Francisco, California 94132, United States;* orcid.org/0000-0001-8930-5297

Neal Border − *Department of Physics and Astronomy, San Francisco State University, San Francisco, California 94132, United States*

Kentaro Yumigeta − *School for Engineering of Matter, Transport and Energy, Arizona State University, Tempe, Arizona 85287, United States*

Mark Blei − *School for Engineering of Matter, Transport and Energy, Arizona State University, Tempe, Arizona 85287, United States*

Sefaattin Tongay − *School for Engineering of Matter, Transport and Energy, Arizona State University, Tempe, Arizona 85287, United States;* orcid.org/0000-0001-8294-984X

K. Watanabe − *National Institute for Materials Science, Tsukuba, Ibaraki 305-0044, Japan;* orcid.org/0000-0003-3701-8119

https://doi.org/10.1021/acs.jpcc.1c10631
J. Phys. Chem. C 2022, 126, 8667−8675

T. Taniguchi − *National Institute for Materials Science, Tsukuba, Ibaraki 305-0044, Japan;* orcid.org/0000-0002-1467-3105

Andrew Ichimura − *Department of Chemistry and Biochemistry, San Francisco State University, San Francisco, California 94132, United States;* orcid.org/0000-0002-7826-102X

Santosh KC − *Chemical and Materials Engineering, San Jose State University, San Jose, California 95112, United States*

Taha Salavati-fard − *School of Chemical, Biological and Materials Engineering, University of Oklahoma, Norman, Oklahoma 73019, United States;* orcid.org/0000-0002-2830-1855

Bin Wang − *School of Chemical, Biological and Materials Engineering, University of Oklahoma, Norman, Oklahoma 73019, United States;* orcid.org/0000-0001-8246-1422

Complete contact information is available at: https://pubs.acs.org/10.1021/acs.jpcc.1c10631

Notes

The authors declare no competing financial interest.

■ ACKNOWLEDGMENTS

We thank Bryce Baker for helping us measure the PL scanning of samples. G.B., V.Z.C., N.B., and A.K.M.N. acknowledge the support from the Department of Defense Award (ID: 72495RTREP). A.K.M.N. also acknowledges the support from the National Science Foundation Grant ECCS-1708907 and the faculty start-up grant provided by the College of Science and Engineering at San Francisco State University. S.KC. acknowledges the faculty start-up grant provided by the Davidson College of Engineering at San Jose State University. Part of this research used resources of the National Energy Research Scientific Computing Center (NERSC), a U.S. Department of Energy Office of Science User Facility located at Lawrence Berkeley National Laboratory, operated under Contract No. DE-AC02-05CH11231 and Extreme Science and Engineering Discovery Environment (XSEDE), which is supported by National Science Foundation Grant Number ACI-1548562. T.S. and B.W. are supported by Basic Energy Sciences, Office of Science, Department of Energy (Grant No. DE-SC0020300). S.T. acknowledges support from NSF CMMI-1933214, NSF DMR-2111812, CMMI-2129412, and NSF ECCS-2052527 as well as DOE-SC0020653. All AFM measurements were supported by NSF for instrumentation facilities (NSF MRI-CMMI 1626611). All Raman spectroscopy data were acquired at the Stanford Nano Shared Facilities (SNSF), supported by the National Science Foundation under award ECCS-2026822.

■ REFERENCES

(1) Wang, Q. H.; Kalantar-Zadeh, K.; Kis, A.; Coleman, J. N.; Strano, M. S. Electronics and optoelectronics of two-dimensional transition metal dichalcogenides. *Nat. Nano* **2012**, *7* (11), 699−712.

(2) Mak, K. F.; Shan, J. Photonics and optoelectronics of 2D semiconductor transition metal dichalcogenides. *Nat. Photon* **2016**, *10* (4), 216−226.

(3) Xia, F.; Wang, H.; Xiao, D.; Dubey, M.; Ramasubramaniam, A. Two-dimensional material nanophotonics. *Nat. Photon* **2014**, *8* (12), 899−907.

(4) Duan, X.; Wang, C.; Pan, A.; Yu, R.; Duan, X. Two-dimensional transition metal dichalcogenides as atomically thin semiconductors: opportunities and challenges. *Chem. Soc. Rev.* **2015**, *44* (24), 8859−8876.

(5) Jariwala, D.; Sangwan, V. K.; Lauhon, L. J.; Marks, T. J.; Hersam, M. C. Emerging Device Applications for Semiconducting Two-Dimensional Transition Metal Dichalcogenides. *ACS Nano* **2014**, *8* (2), 1102−1120.

(6) Manzeli, S.; Ovchinnikov, D.; Pasquier, D.; Yazyev, O. V.; Kis, A. 2D transition metal dichalcogenides. *Nature Reviews Materials* **2017**, *2*, 17033.

(7) Zhu, Z. Y.; Cheng, Y. C.; Schwingenschlögl, U. Giant spin-orbit-induced spin splitting in two-dimensional transition-metal dichalcogenide semiconductors. *Phys. Rev. B* **2011**, *84* (15), 153402.

(8) Sun, L.; Yan, J.; Zhan, D.; Liu, L.; Hu, H.; Li, H.; Tay, B. K.; Kuo, J.-L.; Huang, C.-C.; Hewak, D. W.; et al. Spin-Orbit Splitting in Single-Layer MoS_2 Revealed by Triply Resonant Raman Scattering. *Phys. Rev. Lett.* **2013**, *111* (12), 126801.

(9) Alidoust, N.; Bian, G.; Xu, S.-Y.; Sankar, R.; Neupane, M.; Liu, C.; Belopolski, I.; Qu, D.-X.; Denlinger, J. D.; Chou, F.-C.; et al. Observation of monolayer valence band spin-orbit effect and induced quantum well states in MoX_2. *Nat. Commun.* **2014**, *5* (1), 4673.

(10) Molina-Sanchez, A.; Sangalli, D.; Hummer, K.; Marini, A.; Wirtz, L. Effect of spin-orbit interaction on the optical spectra of single-layer, double-layer, and bulk MoS_2. *Phys. Rev. B* **2013**, *88* (4), 045412.

(11) Cheiwchanchamnangij, T.; Lambrecht, W. R. L. Quasiparticle band structure calculation of monolayer, bilayer, and bulk MoS_2. *Phys. Rev. B* **2012**, *85* (20), 205302.

(12) Latzke, D. W.; Zhang, W.; Suslu, A.; Chang, T.-R.; Lin, H.; Jeng, H.-T.; Tongay, S.; Wu, J.; Bansil, A.; Lanzara, A. Electronic structure, spin-orbit coupling, and interlayer interaction in bulk MoS_2 and WS_2. *Phys. Rev. B* **2015**, *91* (23), 235202.

(13) Zhang, Y.; Li, H.; Wang, H.; Liu, R.; Zhang, S.-L.; Qiu, Z.-J. On Valence-Band Splitting in Layered MoS_2. *ACS Nano* **2015**, *9* (8), 8514−8519.

(14) Mak, K. F.; He, K.; Shan, J.; Heinz, T. F. Control of valley polarization in monolayer MoS_2 by optical helicity. *Nat. Nano* **2012**, *7* (8), 494−498.

(15) Bhowal, S.; Satpathy, S. Intrinsic orbital and spin Hall effects in monolayer transition metal dichalcogenides. *Phys. Rev. B* **2020**, *102* (3), 035409.

(16) Zhou, B. T.; Taguchi, K.; Kawaguchi, Y.; Tanaka, Y.; Law, K. T. Spin-orbit coupling induced valley Hall effects in transition-metal dichalcogenides. *Communications Physics* **2019**, *2* (1), 26.

(17) Cao, T.; Wang, G.; Han, W.; Ye, H.; Zhu, C.; Shi, J.; Niu, Q.; Tan, P.; Wang, E.; Liu, B.; Feng, J. Valley-selective circular dichroism of monolayer molybdenum disulphide. *Nat. Commun.* **2012**, *3*, 887.

(18) Dou, X.; Ding, K.; Jiang, D.; Fan, X.; Sun, B. Probing Spin−Orbit Coupling and Interlayer Coupling in Atomically Thin Molybdenum Disulfide Using Hydrostatic Pressure. *ACS Nano* **2016**, *10* (1), 1619−1624.

(19) Klots, A. R.; Newaz, A. K. M.; Wang, B.; Prasai, D.; Krzyzanowska, H.; Lin, J.; Caudel, D.; Ghimire, N. J.; Yan, J.; Ivanov, B. L.; et al. Probing excitonic states in suspended two-dimensional semiconductors by photocurrent spectroscopy. *Sci. Rep.* **2015**, *4*, 6608.

(20) Freitag, M.; Low, T.; Xia, F.; Avouris, P. Photoconductivity of biased graphene. *Nat. Photonics* **2013**, *7* (1), 53−59.

(21) Konstantatos, G.; Badioli, M.; Gaudreau, L.; Osmond, J.; Bernechea, M.; de Arquer, F. P. G.; Gatti, F.; Koppens, F. H. L. Hybrid graphene-quantum dot phototransistors with ultrahigh gain. *Nat. Nano* **2012**, *7* (6), 363−368.

(22) Kresse, G.; Furthmüller, J. Efficient iterative schemes for ab initio total-energy calculations using a plane-wave basis set. *Phys. Rev. B* **1996**, *54* (16), 11169−11186.

(23) Kresse, G.; Furthmüller, J. Efficiency of ab-initio total energy calculations for metals and semiconductors using a plane-wave basis set. *Comput. Mater. Sci.* **1996**, *6* (1), 15−50.

(24) Blöchl, P. E. Projector augmented-wave method. *Phys. Rev. B* **1994**, *50* (24), 17953−17979.

(25) Perdew, J. P.; Burke, K.; Ernzerhof, M. Generalized Gradient Approximation Made Simple. *Phys. Rev. Lett.* **1996**, *77* (18), 3865−3868.
(26) Onida, G.; Reining, L.; Rubio, A. Electronic excitations: density-functional versus many-body Green's-function approaches. *Rev. Mod. Phys.* **2002**, *74* (2), 601−659.
(27) Mortensen, J. J.; Hansen, L. B.; Jacobsen, K. W. Real-space grid implementation of the projector augmented wave method. *Phys. Rev. B* **2005**, *71* (3), 035109.
(28) Enkovaara, J.; Rostgaard, C.; Mortensen, J. J.; Chen, J.; Dułak, M.; Ferrighi, L.; Gavnholt, J.; Glinsvad, C.; Haikola, V.; Hansen, H. A.; et al. Electronic structure calculations with GPAW: a real-space implementation of the projector augmented-wave method. *J. Phys.: Condens. Matter* **2010**, *22* (25), 253202.
(29) Huser, F.; Olsen, T.; Thygesen, K. S. How dielectric screening in two-dimensional crystals affects the convergence of excited-state calculations: Monolayer MoS_2. *Phys. Rev. B* **2013**, *88* (24), 245309.
(30) Mak, K. F.; Lee, C.; Hone, J.; Shan, J.; Heinz, T. F. Atomically Thin MoS_2: A New Direct-Gap Semiconductor. *Phys. Rev. Lett.* **2010**, *105* (13), 136805.
(31) Qiu, D. Y.; da Jornada, F. H.; Louie, S. G. Optical Spectrum of MoS_2: Many-Body Effects and Diversity of Exciton States. *Phys. Rev. Lett.* **2013**, *111* (21), 216805.
(32) Ci, P.; Chen, Y.; Kang, J.; Suzuki, R.; Choe, H. S.; Suh, J.; Ko, C.; Park, T.; Shen, K.; Iwasa, Y.; et al. Quantifying van der Waals Interactions in Layered Transition Metal Dichalcogenides from Pressure-Enhanced Valence Band Splitting. *Nano Lett.* **2017**, *17* (8), 4982−4988.
(33) Li, X.; Li, J.; Wang, K.; Wang, X.; Wang, S.; Chu, X.; Xu, M.; Fang, X.; Wei, Z.; Zhai, Y.; Zou, B. Pressure and temperature-dependent Raman spectra of MoS2 film. *Appl. Phys. Lett.* **2016**, *109* (24), 242101.
(34) Sahoo, S.; Gaur, A. P. S.; Ahmadi, M.; Guinel, M. J. F.; Katiyar, R. S. Temperature-Dependent Raman Studies and Thermal Conductivity of Few-Layer MoS2. *J. Phys. Chem. C* **2013**, *117* (17), 9042−9047.
(35) Kormányos, A.; Zólyomi, V.; Drummond, N. D.; Burkard, G. Spin-Orbit Coupling, Quantum Dots, and Qubits in Monolayer Transition Metal Dichalcogenides. *Physical Review X* **2014**, *4* (1), 011034.
(36) Le, N. B.; Huan, T. D.; Woods, L. M. Interlayer Interactions in van der Waals Heterostructures: Electron and Phonon Properties. *ACS Appl. Mater. Interfaces* **2016**, *8* (9), 6286−6292.
(37) Bradley, A. J.; Ugeda, M. M.; da Jornada, F. H.; Qiu, D. Y.; Ruan, W.; Zhang, Y.; Wickenburg, S.; Riss, A.; Lu, J.; Mo, S.-K.; et al. Probing the Role of Interlayer Coupling and Coulomb Interactions on Electronic Structure in Few-Layer MoSe2 Nanostructures. *Nano Lett.* **2015**, *15* (4), 2594−2599.
(38) Kc, S.; Longo, R. C.; Addou, R.; Wallace, R. M.; Cho, K. Impact of intrinsic atomic defects on the electronic structure of MoS2monolayers. *Nanotechnology* **2014**, *25* (37), 375703.
(39) Pizarro, J. M.; Rösner, M.; Thomale, R.; Valentí, R.; Wehling, T. O. Internal screening and dielectric engineering in magic-angle twisted bilayer graphene. *Phys. Rev. B* **2019**, *100* (16), 161102.
(40) Ryou, J.; Kim, Y.-S.; Kc, S.; Cho, K. Monolayer MoS2 Bandgap Modulation by Dielectric Environments and Tunable Bandgap Transistors. *Sci. Rep.* **2016**, *6* (1), 29184.
(41) KC, S.; Longo, R. C.; Wallace, R. M.; Cho, K. Computational Study of MoS_2/HfO_2 Defective Interfaces for Nanometer-Scale Electronics. *ACS Omega* **2017**, *2* (6), 2827−2834.

https://doi.org/10.1021/acs.jpcc.1c10631
J. Phys. Chem. C 2022, 126, 8667−8675